Heterostructure-based optical absorbers

Gui-qiang Du,[1,2] Hai-tao Jiang,[1,3,*] Zhan-shan Wang,[1,3] Ya-ping Yang,[1,3] Zi-li Wang,[1,3] Hai-qing Lin,[4] and Hong Chen[1,3,5]

[1]*Pohl Institute of Solid State Physics, Tongji University, Shanghai 200092, China*
[2]*School of Space Science and Physics, Shandong University at Weihai, Weihai 264209, China*
[3]*Shanghai Key Laboratory of Special Artificial Microstructure Materials and Technology, Tongji University, Shanghai 200092, China*
[4]*Department of Physics, The Chinese University of Hong Kong, Shatin, Hong Kong, China*
[5]*E-mail: hongchen@tongji.edu.cn*
[*]*Corresponding author: jiang-haitao@tongji.edu.cn*

Received April 2, 2010; revised June 16, 2010; accepted July 13, 2010;
posted July 16, 2010 (Doc. ID 126216); published August 12, 2010

We have fabricated optical absorbers based on heterostructures composed of thick metallic films and truncated all-dielectric photonic crystals. Under the tunneling mechanism, the light can enter the heterostructure without reflection and is greatly absorbed due to the strong local-field enhancement in the metallic film. With the increase in the thickness of the metal, the absorbance will tend to unity. Experiments, in good agreement with the simulations, demonstrate a maximum of absorbance close to 98%. Possible methods to realize a wide-angle or/and wideband absorption are also given. © 2010 Optical Society of America

OCIS codes: 160.5298, 160.3918, 350.2450.

1. INTRODUCTION

Perfect optical absorbers are highly desirable in many applications such as in the conversion of solar energy, the detector of photonic radiation, the thermal light-emitting sources, etc. [1]. However, it is not easy to realize total absorption since strong reflection always occurs at the surface of a material with a high loss. In microwave and terahertz regions, metamaterial absorbers based on metallic resonant unit cells have been achieved [2–5]. In the visible region, although metals have larger absorption coefficients than those of ordinary dielectrics, metals are nice mirrors instead of good absorbers. A unit structure with metal and dielectric layers can reduce the reflection through resonance or an anti-reflection layer. However, the thickness of the absorbing metal layer is thin (in the scale of one skin depth) and usually the node of the electric field locates at the metal, which limits the absorption efficiency. Cascading this layered unit structure into a one-dimensional metal-dielectric (quasi-)periodic structure or fabricating a graded-index layer on top of the metal can improve the absorption efficiency [6–12]. On the other hand, a nanostructured metal with grating at the surface or an array of tiny dielectric (air) spheres embedded beneath the surface can strongly absorb light via the excitation of some kinds of resonances. For metallic gratings, the grating at the surface of the metal can change the in-plane wave vectors and thus can excite the surface plasmon-polaritons to couple the light into the metal [13,14]. For metals structured by nanocavities, enhanced absorption is triggered by void plasmonic resonance [15], cavity resonance [16], or the coupling of plasmonic and cavity resonances [17]. The key point of above methods is to couple the light into the metal and greatly enhance the local fields by introducing microstructures at or near the surface of the metal. Generally, it is not easy to fabricate nanostructured metals. Can we realize strong local-field enhancement in a thick metal without any microstructure in it to induce strong absorption based on another mechanism?

In 2003, it was found that electromagnetic (EM) waves can tunnel through a heterostructure composed of a ε-negative (ENG) material ($\varepsilon<0,\mu>0$) and a μ-negative (MNG) material ($\varepsilon>0,\mu<0$) under the impedance and the phase matching conditions [18]. The EM fields of the tunneling mode are localized at the interface between the two kinds of materials. Distinct from the conventional surface plasmon-polaritons, this tunneling mode (also called Tamm plasmon-polaritons [19]) can be excited when the in-plane wave vector lies inside the light cone of air. Recently, photonic crystals (PhCs) are shown to have the effect of a MNG material that is rather difficult to realize in the visible region [20–22]. Particularly, tunneling modes for visible light can appear in a heterostructure composed of a metallic film with negative permittivity and a truncated PhC that plays the role of a MNG material. These tunneling modes provide us another way to directly couple the light into the metal. In this paper, we demonstrate that the light of the tunneling mode can enter the heterostructure without reflection and is almost totally absorbed due to the strong local-field enhancement in the intact metallic film.

The paper is organized as follows. In Section 2, we analytically deduce the conditions for the appearance of tunneling mode in the heterostructure. In Section 3, we measure the reflectance, the transmittance, and the absorbance spectra of heterostructures. Particularly, we study the variance of the absorbance with the thickness of the metal layer. Then, possible methods to realize a wide-angle or/and wideband absorption are given. Finally, we conclude in Section 4.

2. CONDITIONS FOR THE TUNNELING MODE

A schematic of the heterostructure denoted by $A(DC)^N$ is shown in Fig. 1(a), where A denotes a metal and $(DC)^N$ represents a PhC with N periods. Normal incidence is considered. Below the plasma frequency, the wave vector and characteristic impedance of the metal are $k_A=(\omega/c)\sqrt{\varepsilon_A\mu_A}=k_{Ar}+ik_{Ai}$ and $\eta_A=\sqrt{\mu_A/\varepsilon_A}=\eta_{Ar}+i\eta_{Ai}$, respectively, where ε_A is the permittivity and the permeability μ_A is 1. At first, we consider the lossless metal. We can obtain $k_A=ik_{Ai}$ and $\eta_A=i\eta_{Ai}$. When the thickness of metal (d_A) is much larger than the skin depth, its wave impedance Z_A can be written as $Z_A=Z_{Ar}+Z_{Ai}i\approx i\eta_{Ai}$. On the other hand, in the gap of the PhC, the Bloch wave vector K satisfies $K\Lambda=m\pi+iK_i\Lambda$ [23], where Λ is the thickness of one period and m is an integer. Besides, in the gap, the wave impedance of the PhC can be obtained as $Z=Z_r+Z_ii=Z_0(1+r/1-r)$ [24], where Z_0 is the wave impedance in the air and r is the reflection coefficient at the entrance face of the PhC that can be described with $r=|r|e^{i\phi}$ ($|r|\approx1$). If ϕ belongs to $[(2m+1)\pi,(2m+2)\pi]$, $Z\approx Z_ii$. Moreover, if N of the PhC is large enough, the characteristic impedance can be replaced with the wave impedance, and K can be taken as the wave vector of an effective medium with the thickness of $N\Lambda$. Based on the above analysis, if zero reflection at entrance face of $A(DC)^N$ occurs [25], an approximate equation is obtained as follows:

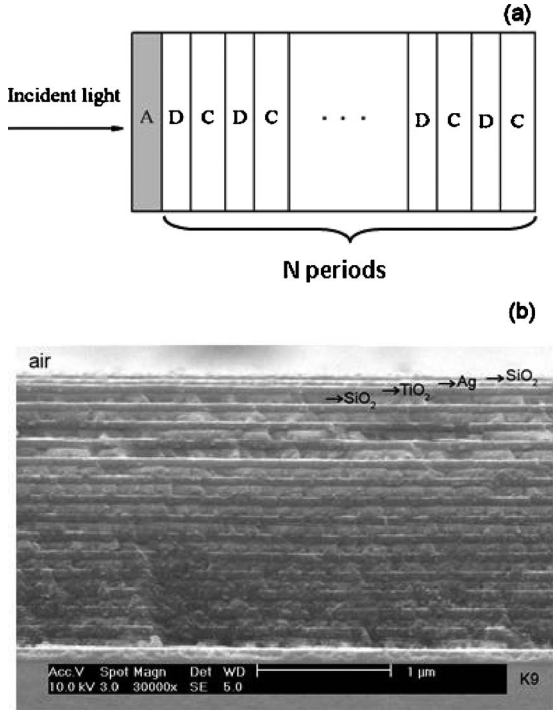

Fig. 1. (a) Schematic of heterostructure $A(DC)^N$, where A denotes metal and $(DC)^N$ represents PhC with N periods. (b) SEM image of the sample $BA(DC)^{15}S$. From top to bottom, $n_B=1.46$, $d_B=50$ nm, $d_A=56.97$ nm, $n_D=2.13$, $d_D=62.68$ nm, $n_C=n_B$, $n_Cd_C=n_Dd_D$, and $n_S=1.52$.

$$\left(Z-\frac{1}{Z}\right)\tan NK\Lambda-\left(\eta_{Ai}+\frac{1}{\eta_{Ai}}\right)\tanh k_{Ai}d_A+i\left(\frac{Z}{\eta_{Ai}}+\frac{\eta_{Ai}}{Z}\right)\tan NK\Lambda\tanh k_{Ai}d_A=0. \quad (1)$$

In the gap, since $K=m\pi/\Lambda+iK_i$ and $Z\approx Z_ii$, Eq. (1) can be approximately simplified to

$$Z_i=-\eta_{Ai},\quad NK_i\Lambda=k_{Ai}d_A. \quad (2)$$

Equations (2), similar to the impedance and the phase matching conditions deduced in the heterostructure composed of ENG and MNG media [18], are the conditions for the excitation of tunneling mode in $A(DC)^N$. Considering the loss of metal, k_A and η_A will have real parts and we need to tune the parameters obtained in the lossless case a little bit to meet the zero-reflection condition in the lossy case.

3. FABRICATION AND MEASUREMENT

Based on Eqs. (2), we design the heterostructure. Metal A is chosen to be silver whose refractive indices [26] are referred from Table 1 while dielectrics C and D are selected to be SiO_2 and TiO_2 whose refractive indices are $n_C=1.46$ and $n_D=2.13$, respectively [27]. The thicknesses of the SiO_2 and TiO_2 layers are $d_C=91.44$ nm and $d_D=62.68$ nm, respectively. At these parameters, the wavelength of absorption will locate within the gap of the SiO_2/TiO_2 PhC. In practice, the heterostructure is modulated to $BA(DC)^NS$, where the substrate S is K9 (a kind of glass) with a refractive index of 1.52 and the protection film B with a thickness of 50 nm is SiO_2. A sample $[BA(DC)^{15}S]$ is fabricated by electronic beam evaporation and its scanning electron microscope (SEM) image is shown in Fig. 1(b). From top to bottom, the protection film, the silver film with a thickness of 56.97 nm, and the TiO_2 and SiO_2 films are indicated by arrows, successively. The reflection and transmission spectra of the samples are measured by an ultraviolet-visible-near infrared spectrophotometer whose tolerance of wavelength is ±0.3 nm. The absorbance is calculated from $A=1-R-T$, where R, T, and A are the reflectance, the transmittance, and the absorbance, respectively. The absolute error range of R and T is ±0.003. Figures 2(a)–2(c) give R, T, and A of $BA(DC)^{15}S$ in Fig. 1, respectively. The numerical results shown by the solid lines are obtained by means of the

Table 1. The Refractive Indices of the Silver Film are Provided by Optorun Co., Ltd. [26]

Wavelength (nm)	Real Part of Refractive Index	Extinction Coefficient
500	0.050	2.87
550	0.055	3.32
600	0.060	3.75
650	0.070	4.20
700	0.075	4.62

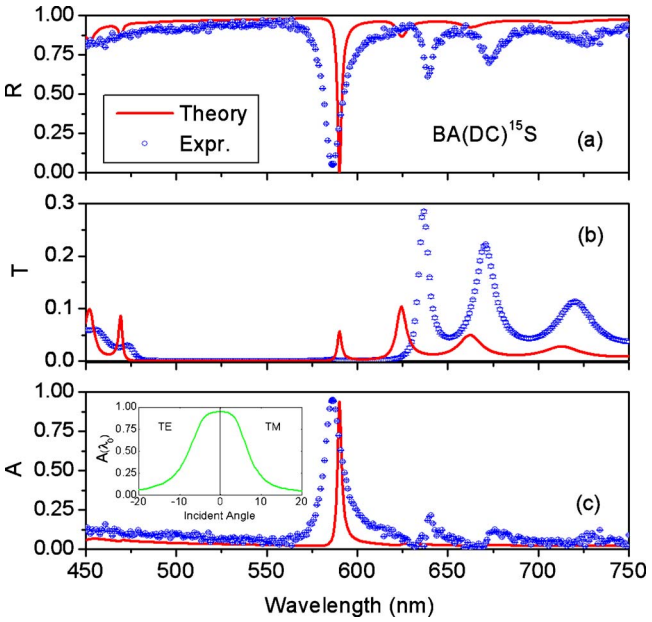

Fig. 2. (Color online) (a), (b), and (c) show R, T, and A of BA(DC)^{15}S, respectively. For numerical values (solid lines), the wavelength of tunneling mode λ_0 is 590.2 nm, and R, T, and A at λ_0 are 4×10^{-8}, 0.0539, and 0.9461, respectively. For measured values (open circles with error bars), λ_0 is 586.6 nm, and R, T, and A at λ_0 are 0.048, 0.003, and 0.949, respectively. Inset shows the simulated angular dependence of the absorbance at λ_0 (590.2 nm) for TE and TM waves.

transfer-matrix method [23]. The wavelength of the tunneling mode (denoted by λ_0) is 590.2 nm, and the reflectance [the dip value in Fig. 2(a)], the transmittance, and the absorbance [the peak value in Fig. 2(c)] at λ_0 are $R=4\times10^{-6}$, $T=0.0539$ and $A=0.9461$, respectively. For the measured values shown by open circles with error bars, λ_0 is 586.6 nm, and R, T, and A at λ_0 are 0.048, 0.003, and 0.949, respectively. The error bars indicate the variation of the reference spectra. The measured results are in good agreement with the simulations although there are slight discrepancies due to the monitoring errors of the layer thickness during the deposition and the difference of refractive indices between theoretical and deposited materials. The inset in Fig. 2(c) shows the simulated angular dependence of the absorbance at λ_0 (590.2 nm) for both transverse electric (TE) and transverse magnetic (TM) waves. The absorbance is nearly invariant within a small angular range, which is similar to that of a metamaterial absorber [2].

Figures 3(a) and 3(b) give the simulated distributions of the intensities of electric field ($|E|^2$) and magnetic field ($|H|^2$) in the sample BA(DC)^{15}S at the wavelength of absorption ($\lambda_0=590.2$ nm) and a wavelength off-absorption ($\lambda_1=540$ nm), respectively. From left to right along the axis of length, the materials are successively the protection film (B), the silver (A), the PhC (DC)^{15}, and the substrate (S). The intensity of the field of the incident wave is supposed to be 1. In Fig. 3(a), the EM fields grow exponentially inside the silver layer at λ_0 (590.2 nm). They are highly localized around the interface between the silver and (DC)^{15}, in which the highest values of $|E|^2$ and $|H|^2$ are 53.51 and 179.43, respectively. This strong local-field

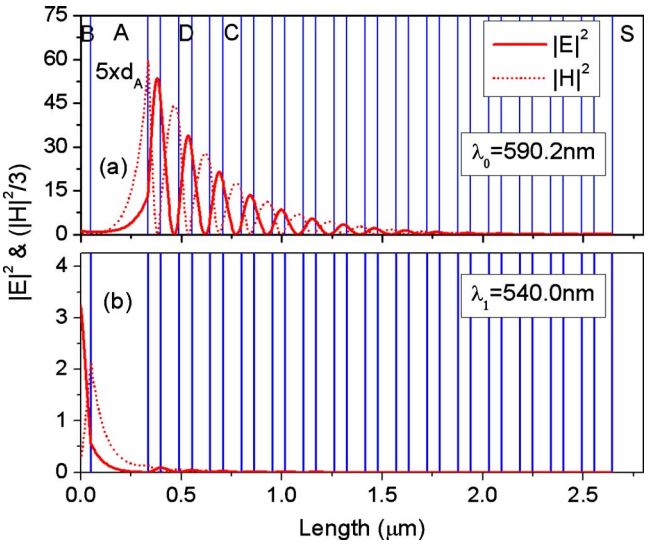

Fig. 3. (Color online) Simulated intensities of the electric (solid line) and magnetic (dotted line) fields in the sample BA(DC)^{15}S at (a) the wavelength of absorption and (b) a wavelength off-absorption. The thickness of Ag in the schematic is five times of its real thickness. All the parameters are the same with those in Fig. 1.

enhancement greatly boosts the absorption of light, while away from 590.2 nm, e.g., at $\lambda_1=540$ nm, the EM fields decay inside the silver as shown in Fig. 3(b) since strong reflection occurs at the entrance face of the structure.

Now we study the variance of absorption with N. We successively increase N from 15 to 21. To meet $NK_i\Lambda=k_{Ai}d_A$ in Eqs. (2), the thicknesses of the silver layer (d_A) are increased to 57.24, 57.42, 57.57, 57.63, 57.68, and 57.71 nm from $N=16$ to 21, respectively, as shown in Fig. 4. All the other parameters are the same with those in the $N=15$ sample. Figure 5 shows the absorbance A of BA(DC)^{N}S with different N in the wavelength range between 570 and 620 nm. The solid lines and circles give the numerical and measured values, respectively. At λ_0, A reaches a peak value for each structure with a given N. Meanwhile, the numerical values of λ_0 for all structures are nearly invariant while the measured λ_0's for $N=18$

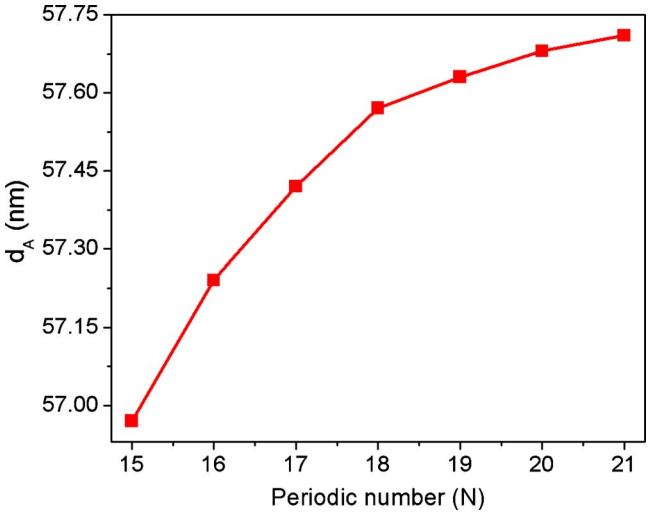

Fig. 4. (Color online) The variance of the thickness of silver layer (d_A) with N.

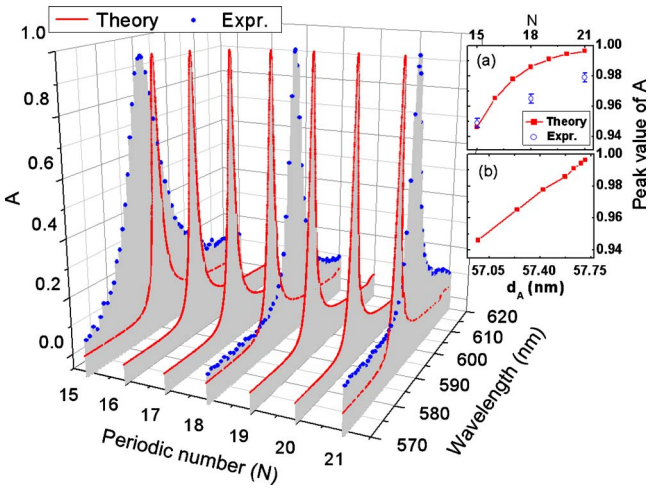

Fig. 5. (Color online) The absorbance A of BA(DC)^{N}S with different N in the wavelength range between 570 and 620 nm. The solid lines and circles give the numerical and measured values, respectively. Insets (a) and (b) show the variances of numerical and measured peak values of A, denoted by solid squares and open circles with error bars, respectively, with N and d_A, respectively. All the other parameters are the same with those in Fig. 1.

and 21 are 599.2 and 597.4 nm, respectively. Insets (a) and (b) in Fig. 5 show the variances of peak values of A with N and d_A, respectively. Both the numerical and measured peak values of A, denoted by solid squares and open circles with error bars, respectively, tend to unity as N or d_A increases. For $N=21$, the numerical and measured peak values of A reach 0.9964 and 0.979, respectively. In fact, since the EM fields in the silver grow exponentially with the length, the absorbance will tend to unity as the length of the silver increases.

From the inset in Fig. 2(c), one can see that the absorption is angle-sensitive. The reason is as follows. It is known that the gap edges of a one-dimensional photonic crystal (1D PhC) will shift noticeably as the angle of incidence varies. Accordingly, the effective parameters retrieved from the gap and the effective Bloch wave vector will change greatly. As a result, if the frequency meeting Eq. (2) at normal incidence is fixed, the value of reflection at the entrance face of the structure will increase noticeably from zero point as the angle of incidence increases. Simultaneously, the absorption will decrease sharply. Therefore, the crucial point to obtain a wide-angle absorption in our structure is to realize an angle-insensitive gap. Since a 2D PhC has more freedom to tune the gap, here we pair a metal with a two-dimensional photonic crystal (2D PhC) instead of a 1D PhC. Figure 6(a) is the schematic of our structure. From the top to bottom, the first layer is the protection film (SiO_2) and the second layer is gold whose refractive indices are referred from [28]. Below the gold layer, there is a truncated 2D PhC with triangle lattices. The 2D PhC is realized by drilling air cylindrical holes inside the background material. Below the truncated 2D PhC, the black zone denotes a substrate that is K9 with a refractive index of 1.52. To get an angle-insensitive gap, the background material in a 2D PhC is supposed to be GaAs whose refractive index is 3.6. The lattice constant of the 2D PhC is 246 nm and the radius of air hole is 111 nm. Supposing a wave with H-polarization,

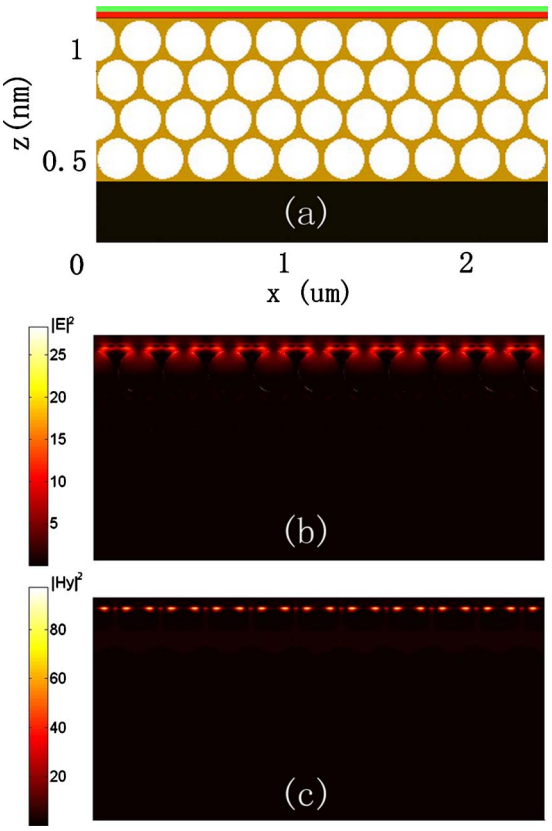

Fig. 6. (Color online) (a) Schematic of a heterostructure composed of a metal and a truncated 2D PhC. From top to bottom, the first layer is protection film (SiO_2) with thickness of 43 nm. The second layer is gold with thickness of 39 nm. Below the gold layer, there is a truncated 2D PhC with triangle lattices. The background material of 2D PhC is GaAs whose refractive index is 3.6. The radius of air hole is 111 nm and the lattice constant of 2D PhC is 246 nm. The thickness of the truncated 2D PhC in z direction is 884 nm. Below the truncated 2D PhC, the black zone denotes substrate that is K9 with refractive index of 1.52. (b) and (c) give the distributions of the intensities of electric and magnetic fields inside the structure shown in (a) at the wavelength of 740 nm for a H-polarized wave, respectively.

i.e., the magnetic field is parallel to the cylindrical hole, in Fig. 7 we calculate the bandgap of the 2D PhC by using a plane wave expansion method [29]. Considering the symmetry of the structure, we only need to calculate the bandgap when the in-plane (x-z plane) wave vector

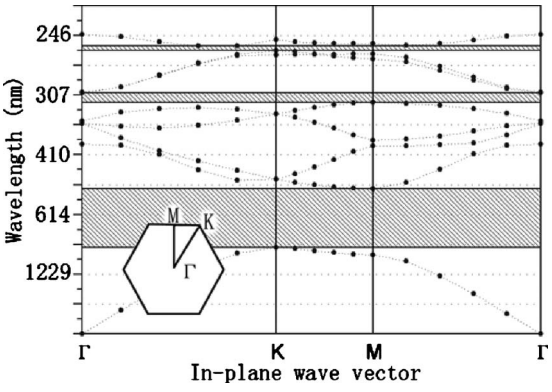

Fig. 7. Diagram of the bandgap of the 2D PhC in Fig. 6(a) when the in-plane wave vector changes in the reduced Brillouin zone in the inset.

changes in the reduced Brillouin zone in the inset (Γ-*K*-*M*-Γ). In Fig. 7, one can see that from *K* to *M*, at the wavelength region from 512 to 847 nm, both the upper and bottom gap edges are nearly flat when the direction of the in-plane wave vector changes by 30°. Considering the symmetry of the Brillouin zone, it means that this gap is almost fixed for all directions of the in-plane wave vector. Then, when the thicknesses of the gold and the protection layer are 39 and 43 nm, respectively, and the thickness of the truncated 2D PhC in the *z* direction is 884 nm, we find the zero reflection at the wavelength of 740 nm inside the gap at normal incidence by using a finite differential frequency domain method [30]. At 740 nm, the permittivity of gold is $-20+1.43i$. Since the thickness of the substrate is on the order of micrometers, it can be considered semi-infinite. Square meshes are used and the size of the computation grid is 1 nm. In *x* and *z* directions, perfectly matched boundaries and periodic boundaries are used, respectively. Moreover, in Figs. 6(b) and 6(c), we calculate the distributions of the intensity of electric and magnetic fields inside the structure, respectively, at the wavelength of 740 nm. It is seen that both electric and magnetic fields are highly localized around the interface of the gold and the truncated 2D PhC. The light will be strongly absorbed due to the enhanced fields in the gold. In Fig. 8, we show the variances of reflectance, transmittance, and absorbance with the angle of incidence at the wavelength of 740 nm. It is seen that even at the incident angle of 60°, the value of absorbance is still nearly 0.8. In other words, a heterostructure composed of a metal and a truncated 2D PhC can obtain a wide-angle absorption.

Here we show that the absorption band can be widened by cascading two heterostructures into a photonic quantum-well structure such as BA′(CD)^{7}A′(CD)^{7}S. The protection film B is TiO_2 with a thickness of 58 nm and S is a substrate K9. Metal A′ is tungsten whose refractive indices are referred from [28] and the thickness of the tungsten layer is 22.5 nm that is nearly 3.5 times of its skin depth at the wavelength of 550 nm. C and D are SiO_2 and TiO_2 whose parameters are the same with those in the former heterostructures. Figures 9(a)–9(c) give the simulated absorption spectra of BA′(CD)^{7}A′(CD)^{7}S at normal incidence and incident angle of 40° for two polarizations, respectively. As shown in Fig. 9, EM waves in a wideband and angle of incidence can enter the structure nearly without reflection and are almost fully absorbed. The physical reason is explained as follows. In the photonic quantum-well structure BA′(CD)^{7}A′(CD)^{7}S, the fields are localized at the two interfaces of the metal film A′ and (CD)^7. If the two interface modes couple with each other strongly, two peaks separated by a frequency interval will appear. But for a weak coupling between two interface modes, two peaks will overlap and merge into a broad band. To strengthen this broadening effect, we choose tungsten that has a larger loss than silver to obtain a relatively wide absorption spectrum for a single heterostructure. Then, when two heterostructures are cascaded into a quantum-well structure, the merged absorption spectrum can be very wide as shown in Fig. 9(a) in the case of normal incidence. Moreover, the quantum-well structure has a good angle-independent response of up to 40° as shown in Figs. 9(b) and 9(c).

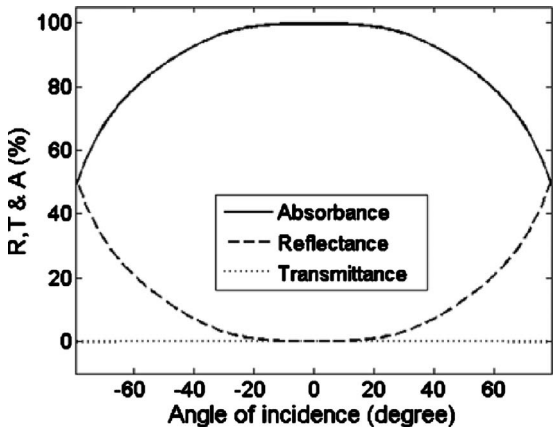

Fig. 8. The variances of reflectance, transmittance, and absorbance of the structure shown in Fig. 6(a) with the angle of incidence at the wavelength of 740 nm.

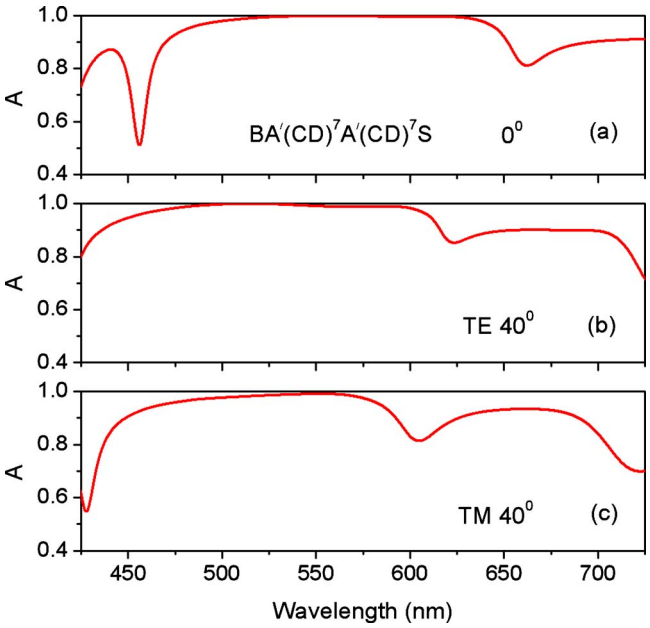

Fig. 9. (Color online) Simulated absorbance *A* of BA′(CD)^{7}A′(CD)^{7}S at normal incidence and incident angle of 40° for two polarizations.

4. CONCLUSION

In conclusion, we theoretically and experimentally demonstrate that light can be strongly absorbed in a heterostructure composed of a thick metallic film and a truncated all-dielectric PhC under a tunneling mechanism. With easy fabrication, these heterostructure-based optical absorbers will play an important role in many applications involving photonic absorption.

ACKNOWLEDGMENTS

This research was supported by the National Basic Research Program of China (Grant No. 2006CB921701), by the National Natural Science Foundation of China (NSFC) (Grants No. 10634050 and No. 10704055), by the Shandong Natural Science Foundation (SDNSF) (Grant

No. Y2008A37), by the Program for Key Basic Research of the Shanghai Science and Technology Committee (Grant No. 08dj1400301), and by the Scientific Research Foundation (SRF) for Returned Overseas Chinese Scholars (ROCS), State Education Ministry (SEM).

REFERENCES AND NOTES

1. Z. P. Yang, L. Ci, J. A. Bur, S. Y. Lin, and P. M. Ajayan, "Experimental observation of an extremely dark material made by a low-density nanotube array," Nano Lett. **8**, 446–451 (2008).
2. N. I. Landy, S. Sajuyigbe, J. J. Mock, D. R. Smith, and W. J. Padillal, "Perfect metamaterial absorber," Phys. Rev. Lett. **100**, 207402 (2008).
3. F. Bilotti, L. Nucci, and L. Vegni, "An SRR based microwave absorber," Microwave Opt. Technol. Lett. **48**, 2171–2175 (2006).
4. H. Tao, N. I. Landy, C. M. Bingham, X. Zhang, R. D. Averitt, and W. J. Padilla, "A metamaterial absorber for the terahertz regime: Design, fabrication and characterization," Opt. Express **16**, 7181–7188 (2008).
5. B. Wang, T. Koschny, and C. M. Soukoulis, "Wide-angle and polarization-independent chiral metamaterial absorber," Phys. Rev. B **80**, 033108 (2009).
6. M. J. Bloemer and M. Scalora, "Transmissive properties of Ag/MgF_2 photonic band gaps," Appl. Phys. Lett. **72**, 1676–1678 (1998).
7. J. F. Yu, Y. F. Shen, X. H. Liu, R. T. Fu, J. Zi, and Z. Q. Zhu, "Absorption in one-dimensional metallic-dielectric photonic crystals," J. Phys. Condens. Matter **16**, L51–L56 (2004).
8. J. W. Dong, G. Q. Liang, Y. H. Chen, and H. Z. Wang, "Robust absorption broadband in one-dimensional metallic-dielectric quasi-periodic structure," Opt. Express **14**, 2014–2020 (2006).
9. M. G. Cappeddu, N. Savalli, S. Baglio, M. Scalora, W. Davenport, M. J. Bloemer, and M. C. Larciprete, "Tunable absorption resonance in electromechanical one-dimensional metallodielectric photonic band gap structures," J. Appl. Phys. **102**, 073531 (2007).
10. H. A. Macleod, ed., *Thin-Film Optical Filters*, 3rd ed. (Institute of Physics, 2001), p. 581.
11. X. F. Li, Y. R. Chen, J. Miao, P. Zhou, Y. X. Zheng, L. Y. Chen, and Y. P. Lee, "High solar absorption of a multilayered thin film structure," Opt. Express **15**, 1907–1912 (2007).
12. I. T. Ritchie and B. Window, "Applications of thin graded-index films to solar absorbers," Appl. Opt. **16**, 1438–1443 (1977).
13. J. Le Perchec, P. Quémerais, A. Barbara, and T. López-Rios, "Why metallic surfaces with grooves a few nanometers deep and wide may strongly absorb visible light," Phys. Rev. Lett. **100**, 066408 (2008).
14. N. Bonod, G. Tayeb, D. Maystre, S. Enoch, and E. Popov, "Total absorption of light by lamellar metallic gratings," Opt. Express **16**, 15431–15438 (2008).
15. T. V. Teperik, F. J. García De Abajo, A. G. Borisov, M. Abdelsalam, P. N. Bartlett, Y. Sugawara, and J. J. Baumberg, "Omnidirectional absorption in nanostructured metal surfaces," Nat. Photonics **2**, 299–301 (2008).
16. N. Bonod and E. Popov, "Total light absorption in a wide range of incidence by nanostructured metals without plasmons," Opt. Lett. **33**, 2398–2400 (2008).
17. G. Sun and C. T. Chan, "Frequency-selective absorption characteristics of a metal surface with embedded dielectric microspheres," Phys. Rev. E **73**, 036613 (2006).
18. A. Alù and N. Engheta, "Pairing an epsilon-negative slab with a mu-negative slab: Resonance, tunneling and transparency," IEEE Trans. Antennas Propag. **51**, 2558–2571 (2003).
19. M. Kaliteevski, I. Iorsh, S. Brand, R. A. Abram, J. M. Chamberlain, A. V. Kavokin, and I. A. Shelykh, "Tamm plasmon-polaritons: Possible electromagnetic states at the interface of a metal and a dielectric Bragg mirror," Phys. Rev. B **76**, 165415 (2007).
20. J. Guo, Y. Sun, Y. W. Zhang, H. Q. Li, H. T. Jiang, and H. Chen, "Experimental investigation of interface states in photonic crystal heterostructures," Phys. Rev. E **78**, 026607 (2008).
21. T. Goto, A. V. Dorofeenko, A. M. Merzlikin, A. V. Baryshev, A. P. Vinogradov, M. Inoue, A. A. Lisyansky, and A. B. Granovsky, "Optical Tamm states in one-dimensional magneto-photonic structures," Phys. Rev. Lett. **101**, 113902 (2008).
22. G. Q. Du, H. T. Jiang, Z. S. Wang, and H. Chen, "Optical nonlinearity enhancement in heterostructures with thick metallic film and truncated photonic crystals," Opt. Lett. **34**, 578–580 (2009).
23. A. Yariv and P. Yeh, eds., *Optical Waves in Crystals* (Wiley, 1984).
24. R. Biswas, Z. Y. Li, and K. M. Ho, "Impedance of photonic crystals and photonic crystal waveguides," Appl. Phys. Lett. **84**, 1254–1256 (2004).
25. K. Busch, C. T. Chan, and C. M. Soukoulis, *Photonic Band Gap Materials* (Kluwer, 1996).
26. Special explanation: since the absorption coefficient of the metallic film is generally smaller than that of bulk metal in [28], we select the refractive indices of silver film in Table 1.
27. J. C. Manifacier, J. Gasiot, and J. P. Fillard, "A simple method for the determination of the optical constants n, h and the thickness of a weakly absorbing thin film," J. Phys. E **9**, 1002–1004 (1976).
28. E. D. Palik, ed., *Handbook of Optical Constants of Solids* (Academic, 1985).
29. J. D. Joannopoulos, R. D. Meade, and J. N. Winn, *Photonic Crystals: Molding the Flow of Light* (Princeton Univ. Press, 1995).
30. C. M. Rappaport and B. J. McCartin, "FDFD analysis of electromagnetic scattering in anisotropic media using unconstrained triangular meshes," IEEE Trans. Antennas Propag. **39**, 345–349 (1991).